20th IMEKO TC10 Conference
"Measurement for Diagnostics, Optimization and Control to Support Competitiveness and Innovation"
Lisbon, Portugal, September 28–29, 2026

Fault location and identification in the RIAA equalizer based on the frequency analysis

Sadhusaran Prasad[1], Grzegorz Makarewicz[1], Piotr Bilski[1]

[1] *Institute of Radioelectronics and Multimedia Technology, Warsaw University of Technology, Warsaw, Poland, s.prasad@student.uw.edu.pl, grzegorz.makarewicz@pw.edu.pl, piotr.bilski@pw.edu.pl*

***Abstract* – The paper presents the approach to diagnose the RIAA equalizer, which is widely used in the high quality audio industry during the music recording. As the circuit is discrete, it is possible to select the partially accessible nodes for response measurement, therefore analysis of their usefulness for the fault location and identification. The cumulative power of the response at each node was used as the source of diagnostic information. Three classifiers (i.e. decision tree, multilayered perceptron and the gaussian Naïve Bayes Classifier) have been used to identify the faults. Conclusions from the experiments show that it is possible to diagnose the audio circuit using the minimal information.**

***Keywords* – RIAA equalizer, fault identification and location, artificial intelligence**

I. INTRODUCTION

Despite the advancement in digital technologies, analog electronics is still in use, preferred in specific applications. The important one is the audio technology, where traditional, vacuum tubes or bipolar transistors provide desired quality of sound and operation of the devices such as amplifiers or correctors [1]. Such solutions are expensive (each element must be of high quality, i.e. low tolerance), which makes their diagnostics critical, as it is hardly practical (due to high costs) to replace the broken circuit with the new, correctly operating one [2]. Therefore the source of the problem should be identified and processed.

Modern diagnostic approaches rely on the Artificial Intelligence (AI), due to their high accuracy and ability to extract relevant information from the available data. This allows for the semi-automated procedures during the fault detection and location. The selected and optimized AI-based classifiers may be used to point at the faulty element, processing features of the signal responses generated after exciting the circuit with the excitation at the accessible (input) node. The classification accuracy depends on knowledge extracted from the circuit model simulations. The important part of the classifier application is its optimization, which is usually implemented in the offline mode [3]. The particular hyperparameters depend on the selected algorithm and require repeated training-testing cycles for their different values (such as number of neurons inside the layer or the maximal depth of the tree).

Although recently multiple deep learning approaches have been proposed also for the technical diagnostics [4], their usefulness is limited. Specifically, when the available data are too small (in case of less popular Systems Under Test - SUTs), the traditional approaches, where the features are first extracted from the raw measurements and the classifier is processing vector of features, are still attractive.

The aim of the following paper is to present the diagnostic analysis of the RIAA corrector used during the high quality audio recording. Three AI-based classifiers, i.e. decision tree (DT), multilayered perceptron (MLP) and Naïve Bayes Classifier (NBC) were used to locate and identify parametric faults. They operate on the simple set of features extracted from the frequency characteristics of the response signals measured at partially accessible nodes. Two tasks, i.e. fault location and fault identification were considered.

The content of the paper is as follows. In Section II the analyzed circuit is described. Section III covers the experimental setup (data set, range of classifiers and their work regime). In Section IV experimental results, covering fault identification and location accuracy, and process of their optimization is presented. The work is concluded with summary and future prospects.

II. SYSTEM UNDER TEST

The presented SUT [5] belongs to the high quality audio devices, used during recording of music media, such as vinyl disks. The process requires constant correction of the frequency characteristics to ensure the appropriate quality for the sophisticated listener. In such scenarios the digital integrated circuits are usually not enough, allowing their discrete analog counterparts to take over. Though such solutions are expensive, they must be used if the sound quality is supposed to meet the audiophile society standards. The structure of the system is presented in Fig. 1, with five partially accessible nodes (i.e. the ones where measurements may be taken) encircled. The node No. 5 is the output one, essential for the audio processing. The circuit is a passive filter, consisting of 12 elements: six resistors (indicated from R_1 to R_6) and six capacitors (indicated from C_1 to C_6).

The structure of the circuit reflects the actual construction requirements. Due to the specific connections between some elements (for instance capacitors C_2 and $C3$, and C_5 and C_6, respectively) might be difficult to distinguish, forming ambiguity groups [6]. This should be visible in the classification results (see Section IV).

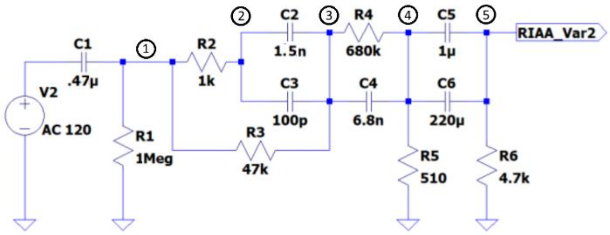

Fig. 1. Topology of the analyzed RIAA corrector

Parameters of the corrector, crucial for the its frequency operation, are represented by the transfer function *F(s)*, with T_1, T_2 and T_3 being the normalized time constants, determining properties of the filter.

$$F(s) = \frac{(s \cdot T_1+1)\cdot(s \cdot T_3+1)}{s \cdot T_2+1} \tag{1}$$

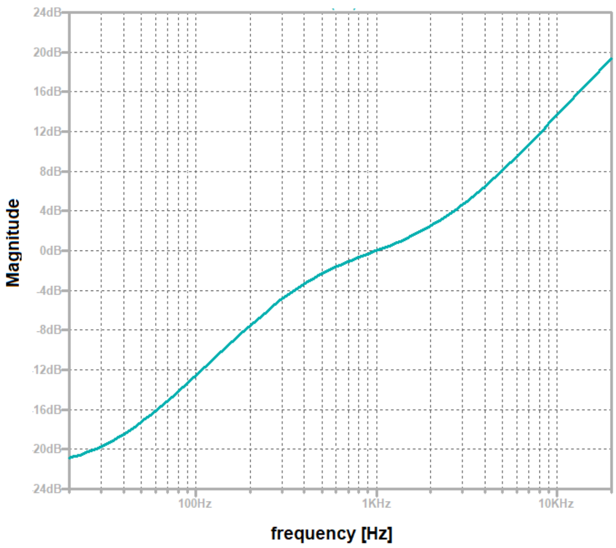

Fig. 2. Nominal audio correction characteristics

The ideal correction characteristics from Fig. 2 represents the transfer function (1) with three folding points, each modeled by the single filter. They define amplitude suppression at 50Hz, 500Hz and 2122Hz, respectively. Characteristics measured at each node represent the highpass band of different shapes (which depend on the values of the internal elements).

The nominal values of the elements were as follows: C1=0.47uF, C2=1.5nF, C3=100pF, C4=6.8nF, C5=1uF, C6=220uF, R1=1MΩ, R2=1kΩ, R3=47kΩ, R4=680kΩ, R5= 510Ω and R6=4.7kΩ.

Amplitude and phase characteristics are obtained after exciting the SUT with the sinusoidal pattern with the amplitude of 100mV and frequency ranging from 20Hz to 20kHz. Example of the highpass amplitude spectrum measured at the node No 3 is in Fig. 3.

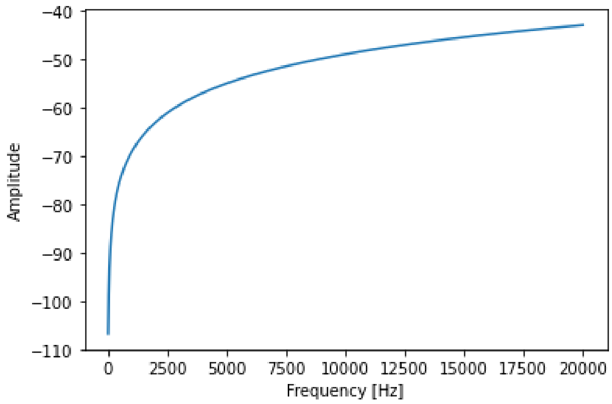

Fig. 3. Amplitude characteristics of the RIAA circuit observed at the output node

III. EXPERIMENTAL SETUP

This section contains description of the framework prepared to analyze the circuit. It uses AI-based algorithms, trained on the available simulation data, and then tested on selected diagnostic cases. All experiments have been conducted in the Python language with the scikit-learn library as the source of the classifiers.

A. Training dataset

The model of the RIAA corrector has been extensively simulated in the LTSpice environment [7]. For each experiment a single parameter (value of resistance or capacitance) was changed beyond the nominal state. The tolerance margins assumed for the model were 10% (i.e. between -5% and 5%) for each element (which is the low acceptance boundary for the high-quality audio equipment). This way 20 simulations were conducted for the subsequent element. The nominal state was emulated with the nominal values of elements disturbed by the random variables within the tolerance margins. Based on the information about the actual value the fault code was assigned (see Section III.C). This way the raw data set *R* with amplitude and phase samples for 240 simulations was created. Besides the presented experiments, it is to be used for future research.

The feature dataset *D* being the base for the presented experiments was constructed using attributes extracted from the spectral characteristics of responses observed at each partially accessible node (indexed 1 to 5 in Fig. 1). The idea was to apply the simplest scheme possible with the minimal number of features for each diagnostics case.

$$a_i = \sum_{j=1}^{N} |f_j|, \quad i=1,\ldots 5 \tag{2}$$

where f_j is the amplitude spectrum sample. This way each example is the following vector:

$$\boldsymbol{x}_k = [a_1 \quad \ldots \quad a_5 \quad c] \tag{3}$$

with c being the fault code.

B. Applied classifiers

Three classifiers have been selected for the experiment, allowing for comparing their efficiency on the same training data. They were selected due to the different form of stored knowledge, which allows for determining the optimal type of algorithm to tackle the feature vectors. Below their short description is provided.

a. DT is the rule-based approach, building the category separation ability on the tests inside the tree structure. Its advantages include simplicity and legibility for the human operator. The verified hyperparameter was the maximum depth of the tree, influencing the ability to avoid overfitting [8].
b. MLP is the most popular "shallow" type of the feed-forward neural network. Knowledge stored in the arrays of weights connecting neurons between layers I difficult to interpret by the human being. Hyperparameters include the number of layers and the number of neurons in each layer [9].
c. NBC is the simple classifier making decisions based on the probabilities of examples having the particular values of features. Because the latter are continuous, gaussian variant of the algorithm was used (assuming their normal distribution). The Gaussian distribution smoothing is the hyperparameter here [10].

Quality of the classifiers was verified using accuracy, being the ratio of correctly identified faults against all present cases.

C. Diagnostic frameworks

Two types of experiments were conducted using the applied classifiers, differing in the fault codes assigned to the examples. In the first one, the aim was the fault location, i.e. finding the faulty element based on the available features. Here the fault code was covered thirteen integers: "0" for the nominal state, and "1" to "12", representing the subsequent elements (i.e. resistors R_1 to R_6 and capacitors C_1 to C_6, respectively). For instance, fault of resistor R_3 is labeled as "3", while fault of capacitor C_2 is indicated by the code "8".

The second task was the fault identification, i.e. determining which element is the source of the fault and its actual state (larger than, represented by the negative identifier, and lesser than the nominal - through the positive identifier). This way the number of codes is doubled (i.e. "-12", "-11", …, "11", "12"), with "0", as before, being the nominal state code. This way too small value of capacitor C_1 is indicated as "-7", while its too large value is labeled as "7".

To confirm the efficiency of both approaches and their independence from the available data, cross-validation was used. The repeated stratified hold-out validation procedure was used. In each trial, the dataset was divided into 70% (i.e. 168) training examples with 30% (i.e. 72) as the testing ones. Stratification was used to preserve distribution of fault categories in both subsets. Cross-validation was repeated 30 times using different random splits. Results presented in Section IV are then average values with standard deviations representing the dispersion of accuracy around the most common values.

IV. EXPERIMENTAL RESULTS

Three classifiers trained on the subsets of the data set *D* were evaluated regarding their accuracy for two variants of fault categories description (location and identification). Each algorithm has been optimized regarding hyperparameters described in Section III.B. Finally, the minimization of sets of nodes has been performed. It is aimed finding the minimal set of nodes allowing for extracting enough information to maintain the diagnostic accuracy [11].

A. Diagnostic accuracy

Compared classifiers show maximum accuracy around 60% in both fault location and identification task. As the reference level is 2.5 % (assuming each category is equally probable), the result is initially acceptable. The best outcomes are reached in both tasks by DT, with remaining classifiers falling significantly behind. Overall results are in Table 1 for identification and in Table 2 for fault location. The worse results for the MLP are probably caused by the insufficient amount of training data, allowing for converging the weight arrays.

Table 1. Optimal average fault identification outcomes for three classifiers

Classifier	Optimal configuration	Accuracy	Standard deviation
DT	Depth = 5	59,35%	3,48%
MLP	Layers: 10:8	41,48%	3,72%
NBC	Smoothing=1e-12	53,84%	4,46%

Comparison between the performance of fault location and identification shows it is easier to perform classification for more categories. This is because in most cases behavior of the SUT for the element values higher than the nominal one is different than for values below the nominal. When such different examples (for instance, labeled as "-5" and "5") are clustered under a single category, the classifier may not be able to bind them. Therefore, for the larger number of categories the tasks remains easier (more groups of similar objects).

Table 2. Optimal average fault location outcomes for three classifiers

Classifier	Optimal configuration	Accuracy	Standard deviation
DT	Depth = 8	57,04%	5,71%
MLP	Layers: 10:6	39,44%	4,42%
NBC	Smoothing=1e-12	47,45%	4,55%

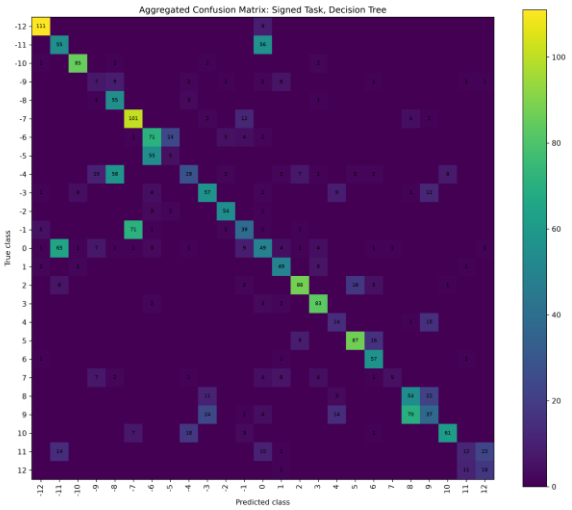

Fig. 4. Confusion matrix for fault identification of the RIAA circuit

The important aspect is the ability to detect and distinguish between the specific faults, learning which ones are the most difficult to identify. Fig. 4 shows the confusion matrix for the DT classifier in the optimal case. Though most elements are mostly distinguishable. In some cases ambiguity groups remain the problem. For instance, too small values of C_5 capacitor are mistaken for the nominal state (which is not a problem as the Sut behaves as if it was working properly). On the other hand, identifications for capacitors C_2 and $C3$ are intertwined (as mentioned earlier, they are indistinguishable due to the position in the circuit structure). In such a case, the manual diagnosis of both elements would be needed. The confusion matrix confirms the possibility of distinguishing between most of the faults, with the mentioned exceptions.

In the case of the fault location the confusion matrix (Fig. 5) is similar with the same detection problems (for instance, capacitors C_2 and C_3 being hardly distinguishable, while faults of C_4 and $C5$ being easily identified). Similarly, the nominal state is sometimes assigned a number of faults that are not visible on the output. This is caused by the low sensitivity of SUT on the changes in selected elements. This should be examined in the future.

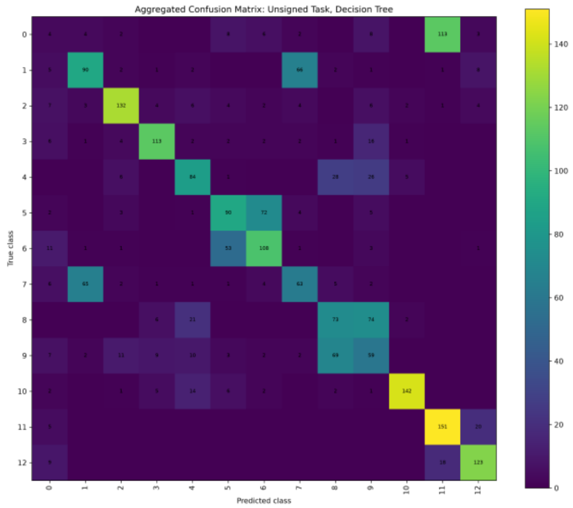

Fig. 5. Confusion matrix for fault location of the RIAA circuit

B. Classifier optimization

Each AI-based classifier is a heuristic approach that provides different outcomes depending on the selected hyperparameters (see Section III.B). The aim of the optimization is to provide the maximum accuracy, independently of the training data. For each classifier a different parameter was tuned, and its best value stored for future use. Note that different values are obtained for two solved tasks.

The DT provided the best performance of fault identification for the tree depth of 5 (leading to the maximum 32 leaves with categories). Increasing the depth makes the tree too complex, not allowing for any improvement. For the fault location the optimal depth is larger (i.e. 8 – see Table 2), which is caused by the greater difficulty in separating objects. This is caused by too crude assignment of fault categories.

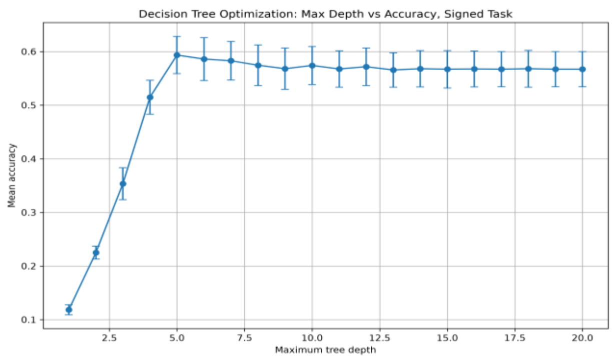

Fig. 6. DT fault identification accuracy as a function of the maximum tree depth

The MLP's accuracy depends on the structure of the network, i.e. the number of neurons, for which the weights are adjusted during the training [12]. Although there are algorithms that modify the network structure during the training, the most typical approach is to build different structures from scratch and perform training-testing routine on them, comparing obtained accuracies. Because of the limited size of the data set and long time of exhaustive simulations, the number of hidden layers was limited to two and the number of neurons in the layer was limited to 30 (with the step of 2). The optimization process is presented in Fig. 7. In general, two hidden layers allowed to obtain better results than a single layer, though if the latter contains large number of neurons (i.e. 30) it provides comparable results to more complex networks.

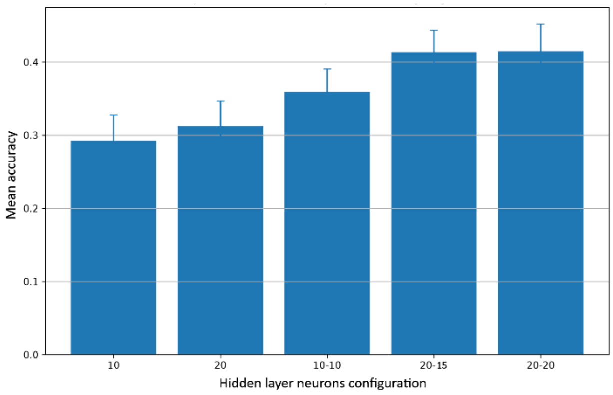

Fig. 7. MLP fault identification accuracy as a function of the neurons structure configuration

Finally, the gaussian NBC smoothing was evaluated. There are two possible implementations of this classifier. The first one is the "traditional", discrete approach, requiring the prior assignment of each attribute's value to the predefined interval. This requires implementing the prior discretization algorithm. The second choice is the operation on the continuous data, with the predefined statistical (here Gaussian) distribution. Behavior of the classifier is similar for both fault identification and location, starting from the high accuracy and going down while increasing the variance of the distribution (Fig. 8).

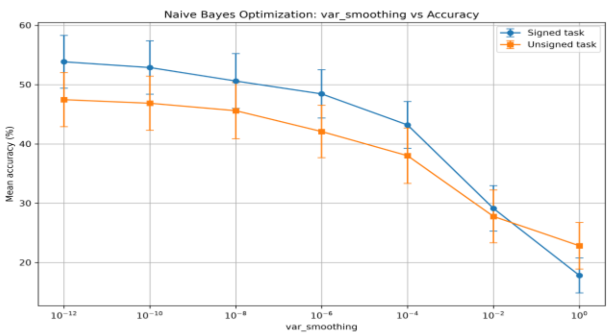

Fig. 8. NBC fault identification and location accuracy as a function of the normal distribution variance smoothing

C. Minimization of nodes

The optimal configuration of DT was used to check possibility of decreasing the number of measurement nodes, maintaining accuracy. The highest score was obtained for data extracted from signals at all five nodes. The procedure to eliminate subsequent nodes (i.e. eliminate attributes from *D*) was applied, with only the fifth (output) one being mandatory. The minimal set was then {5} and maximal one: {1,2,3,4,5}. Only the latter allows for the maximum accuracy, though elimination of some nodes does not degrade the efficiency significantly (Fig. 9). Introducing other attributes from the single measured signal may lead to decreasing number of nodes.

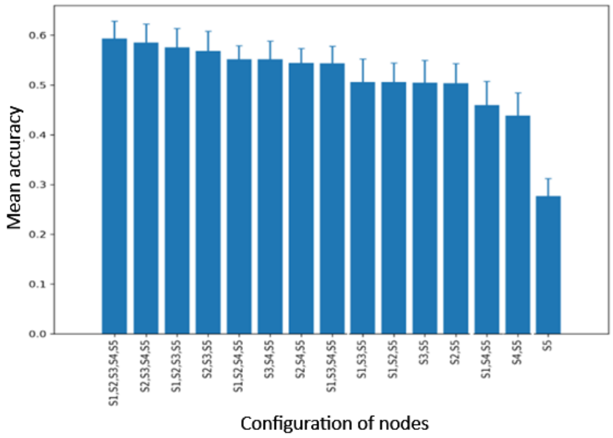

Fig. 9. DT fault identification accuracy as a function of sets of measurement nodes

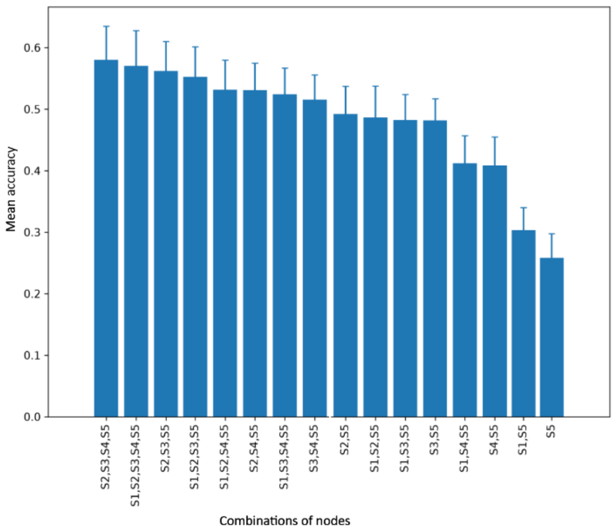

Fig. 10. DT fault location accuracy as a function of sets of measurement nodes

The situation for the fault location is similar, i.e. the highest accuracy is obtained either for the complete set of 5 nodes, or 4 of them, where the node No. 1 has the minimum influence on the overall results, is it is the first in the sequence, therefore changes in most elements are not visible in responses recorded here (Fig. 10). Similarly, using only the output node leads to the lowest accuracy, therefore it is required either to maintain additional nodes as partially accessible, or introduce new attributes representing each response in the set *R*.

V. CONCLUSIONS

The presented analysis showed the approach for the diagnostics of the RIAA corrector based on the spectral characteristics of the signals measured on five partially accessible nodes. Three classifiers were applied to process the dataset containing cumulative amplitude spectra. It was established that such minimal information allows for distinguishing between different faults to some extent, though more precise analysis is required, specifically to increase the overall accuracy. On the other hand, some sets of SUT elements will be difficult to distinguish because of their location in the circuit structure. Detection of ambiguity groups should be incorporated into the designed framework [13].

Future research should include introduction of other features from the spectral characteristics (such as value and frequency of the maximum peak, or the phase features). Also additional classifiers should be used, specifically the ones tackling uncertainty conditions (such as random forest [14] or the support vector machine). Next, the deep learning may be tried for the scheme, operating directly on the raw measurements [4].

The discussed research considered the computer model only. Because the presented research has the wide practical implications, the final verification of the proposed approach will be its implementation to identify faults in the actual, real-world system. Such experiments will allow for the verification of the model accuracy and usefulness of knowledge extracted from the training data set.

REFERENCES

[1] **Singh, B.:** Analog Circuit Design for High-Fidelity Audio Signal Conditioning: A Theoretical and Simulation-Based Performance Evaluation. *Journal of Multidisciplinary Knowledge*. Vol. 6, 2026, pp. 94-101, DOI: 10.36676/jmk.v6.i1.143.

[2] **Golonek T.; Chruszczyk L.:** Analog circuits specification driven testing by means of digital stream and non-linear estimation model optimized evolutionarily, Bulletin Of The Polish Academy Of Sciences: Technical Sciences, Vol. 68, No. 6, 2020, pp. 1283-1299, DOI: 10.24425/bpasts.2020.13539.

[3] **Kunche S.; Chen C., Pecht M. G.:** Optimized diagnostic model combination for improving diagnostic accuracy, 2013, *Processing IEEE Aerospace Conference*, Big Sky, MT, USA, 2013, pp. 1-10, DOI: 10.1109/AERO.2013.6497197.

[4] **Zhao D.; Xing, J.; Wang, Z.**: Analog Circuit Fault Diagnosis Based on Deep Learning, *Proceedings 4th International Conference on Mechanical Materials and Manufacturing Engineering*, 2016, 10.2991/mmme-16.2016.58.

[5] **Makarewicz G.; Bilski P**.: Diagnostics of the RIAA Equalizer in a Turntable Using Artificial Neural Network, 17th IMEKO TC10 Conference, Dubrovnik, CROATIA, 20-22 Oct. 2020.

[6] **Cannas B.; Fanni A.; Montisci A.**: A fast procedure for canonical ambiguity groups determination in nonlinear analog circuits, *Proceedings of 2010 IEEE International Symposium on Circuits and Systems*, Paris, France, 2010, pp. 1539-1542, doi: 10.1109/ISCAS.2010.5537394.

[7] **Gadjeva E.; Iatcheva I.; Petkova N.**: Stability Analysis of Electronic Circuits Using LTSPICE, *Proceedings International Scientific Conference on Computer Science*, Sozopol, Bulgaria, 2023, pp. 1-4, DOI: 10.1109/COMSCI59259.2023.10315842.

[8] **Chen M.; Haggag H.; Orailoglu A.**: Decision tree based mismatch diagnosis in analog circuits, *Proceedings 24th IEEE VLSI Test Symposium*, Berkeley, CA, USA, 2006, pp. 6 pp.-285, DOI: 10.1109/VTS.2006.26.

[9] **Grzechca D.; Rutowski J.; Golonek T.**: Use of the multilayer perceptron to analog fault functional test creation, IFAC Proceedings Volumes, Vol. 39, 2006, pp. 352-355, DOI: 10.1016/S1474-6670(17)30210-0

[10] **Kumar A. N.; Lingaswamy K.; Nagaraju M.; Ramesha M.; Kiran E. U.; Viswanath Allamraju K.**: Naive Bayes Classifier for Cascaded H-Bridge Multi-Level Inverter Open Circuit Fault Diagnosis, *International Conference on Computational Intelligence for Security, Communication and Sustainable Development (CISCSD)*, Port Blair, India, 2024, pp. 252-255, DOI: 10.1109/CISCSD63381.2024.00063.

[11] **Chang, Y.; Xu, X.; Deng, K.; Xu, Y.; Tu, B.; Gao, X.; Wei, Q.**: An Analog Circuit Fault Diagnosis Method Incorporating Multi-Objective Selection of Measurement Nodes. *Electronics* **2025**, No. *14,* 1528, DOI: 10.3390/electronics14081528 .

[12] **Khoualdia T.; Lakehal A.; Chelli Z.; Khoualdia K.; Nessaib K.**: Optimized Multi Layer Perceptron Artificial Neural Network Based Fault Diagnosis Of Induction Motor Using Vibration Signals, *Diagnostyka*, 2021, Vol. 22, No. 1, DOI: 10.29354/diag/133091.

[13] **Bilski P.**: Ambiguity groups detection in analog systems diagnostics using Self-Organizing Maps, *14th IMEKO TC10 Workshop Technical Diagnostics*, Milan, Italy, June 27-28, 2016.

[14] **Chakraborty D.; Sur U.; Banerjee P. K.:** Random Forest Based Fault Classification Technique for Active Power System Networks, *IEEE International WIE Conference on Electrical and Computer Engineering (WIECON-ECE)*, Bangalore, India, 2019, pp. 1-4, doi: 10.1109/WIECON-ECE48653.2019.9019922.